Improving heat transfer of stabilised thermal oil-based tin nanofluids using biosurfactant and molecular layer deposition

Javier Gil-Font[1], Marie-Anne Hatte[1], Maximilian R. Bailey[2,3], Nuria Navarrete[1], Jorge Ventura Espinosa[1], Aristeidis Goulas[2], Damiano La Zara[2], J. Ruud van Ommen[2], Rosa Mondragón[1], Leonor Hernández[1*]

[1] Departamento de Ingeniería Mecánica y Construcción, Universitat Jaume I, 12071-Castellón de la Plana, Spain

[2]Department of Chemical Engineering, Delft University of Technology, 2629 HZ, Delft, the Netherlands.

[3]Laboratory for Soft Materials and Interfaces, Department of Materials, ETH Zürich, 8093 Zürich, Switzerland

**Corresponding author: lhernand@uji.es*

ABSTRACT

The development of advanced heat transfer fluids (HTF) with enhanced heat transfer properties has been identified as a key target to increase the efficiency of industrial processes. In this work, heat transfer performance improvements of a novel nanofluid, consisting of metallic nanoparticles dispersed in a commercial thermal oil, were investigated. Nanofluids combining tin nanoparticles (1 mass %) with Therminol 66 (TH66) were synthesised using the two step-method and experimentally analysed. The effectiveness of biosurfactant addition and nanoparticle polyethylene terephthalate (PET) nanocoating for high temperature nanofluid stabilisation were independently investigated. The PET nanoscale coatings were grown by molecular layer deposition, which has been used for the first time in this field. The thermal conductivity, dynamic viscosity and specific heat capacity of the stable, oil-based nanofluids were characterised at high temperatures, and the results were compared and in good agreement with models found in the relevant literature. Finally, the heat transfer performance of the nanofluids with respect to their base fluids was evaluated, employing empirical values for the thermophysical properties of the involved materials. In this way, increments of the heat transfer coefficients up to 9.3% at 140 ºC, relevant to industrial applications were obtained.

Keywords: Nanofluid; thermal oil; high temperature stability; heat transfer, molecular layer deposition; biosurfactant.

1. Introduction

Increasing the overall efficiencies and reducing the costs of industrial processes have been identified as key targets to address the ongoing climate crisis while maintaining and improving current living standards. The development of advanced heat transfer fluids (HTF) with enhanced heat transfer properties can play an important role in achieving these goals, as heat transfer is involved in most industrial applications. The heat transfer performance of current high temperature HTF is generally poor due to the low thermal conductivity of these fluids. However, the development of nanotechnology enables the dispersal of nanoparticles (less than 100 nm) into HTF to modify their thermophysical properties, providing new opportunities to improve heat transfer performances by developing HTF-based nanofluids [1], [2].

One of the major challenges facing nanofluids is their limited stability, understood as producing and maintaining homogeneous suspensions, at high temperatures. Sedimentation caused by agglomeration of the nanoparticles needs to be avoided prior to any potential industrial application, as the improved properties of homogeneous nanofluids are not maintained if the nanofluid is not stable. Furthermore, agglomeration of a nanofluid can damage equipment in which the nanofluids are utilised. When using non-aqueous media, nanofluids are typically stabilised via surfactant addition to achieve steric repulsion between the nanoparticles. However, the selection of a suitable surfactant is complicated by their decomposition at high temperatures, and their inability to stabilise the nanoparticles under such conditions.

The most studied property of nanofluids is their thermal conductivity, as solid nanoparticles can increase this variable with respect to the HTF base fluid. Nanofluids produced with metallic nanoparticles exhibit significant enhancements in their thermal conductivity, indicating their potential for industries that depend on heat transfer performance, such as heat sinks [3], [4], cooling for electronic devices [5], [6], heat pipes [7], solar collectors [8], concentrated solar power plants [9], etc. Nevertheless, the heat transfer coefficient can depend on other thermophysical properties, namely viscosity and specific heat capacity, that also need to be evaluated to properly assess this coefficient for nanofluid flows [10]. Limited research has been dedicated to improving the thermal performance of medium- to high temperature oil-based nanofluids, as the majority of the literature has focused on water or water-based nanofluids [2], [8], [11]. Another challenge in this case is that, in order to properly evaluate the performance of oil-based nanofluids in heat transfer applications, the thermo-physical properties (at least thermal conductivity and viscosity) should be measured in the medium- to high temperature range of their applications [12].

The nanofluids synthesised and experimentally tested in this study combine a popular commercial organic oil (Therminol 66, TH66) with tin nanoparticles at low mass concentration. The high temperature stability of the nanofluids was evaluated for two different stabilization approaches: the first treating the base fluid through the addition of surfactants, and the second involving the direct coating of the nanoparticles. As in previous studies, where oleic acid was used to stabilise metal oxide nanoparticles in different Therminol oils [13]–[16], in this work different purities of this surfactant to obtain a stable nanofluid were evaluated. Additionally, olive oil (with high concentrations of oleic acid) was tested as a biosurfactant. Utilising biosurfactants is not only desirable due to their widespread availability, but also from an economic perspective [17]. Nanofluid stabilisation via particle coating was also analysed by depositing ultrathin polyethylene terephthalate (PET) films on the tin nanoparticles using molecular layer deposition (MLD). MLD is a vapour phase deposition technique that enables the controlled growth of conformal, ultrathin organic films on a range of substrates [18]. To date, pure-organic MLD literature predominantly consists of fundamental investigations on flat substrates, and demonstrations of the industrial relevance of this technique are limited despite its promising attributes [19], [20]. Here, the MLD-grown PET coating makes the tin nanoparticles chemically compatible with the thermal oil, obviating the need for additional surfactants. The properties of the resulting stable nanofluids, including thermal conductivity, dynamic viscosity and specific heat capacity, were characterised at high temperature. The measured results were analysed and compared with existing models available for these variables in the literature. Based on these measured properties, the heat transfer performance of the nanofluids was assessed.

2. Materials and methods

2.1 Materials

Therminol 66, TH66, (Solutia, Inc.) was used as base fluid to prepare the thermal oil-based nanofluids. It is one of the most commonly used heat transfer fluids for the desired medium-to-high temperatures. The tin (Sn) nanoparticles dispersed in the nanofluid were purchased from US Research Nanomaterials, Inc. with nominal size of < 300 nm. These nanoparticles were already analysed in a previous work [21], with the conclusion that they are composed of a metallic tin core covered by a tin oxide shell, which is naturally formed during the fabrication process due to their exposure to air.

Two different methods were evaluated to stabilise the nanoparticles in the base fluid, both based on the modification of the characteristics of the nanoparticle surface. The presence of an organic structure on the

surface helps to increase the compatibility with the thermal oil and hence the dispersion and stability of the nanoparticles. In the first method, the addition of surfactants such as oleic acid technical grade 90% (Sigma-Aldrich Inc.), oleic acid 97% (Acros Organics) and virgin olive oil (with oleic acid concentrations between 55 to 83% depending on the variety and thermal conditions [22]) as a biosurfactant was investigated. In the second approach, nanoparticles were coated with PET by MLD to modify the chemical composition of the nanoparticle surface, removing the need for surfactant addition during the preparation of the nanofluid. The MLD precursors, terephthaloyl chloride (TC) and ethylene glycol (EG), were purchased from Sigma-Aldrich and used as received.

2.2 Molecular Layer Deposition (MLD) coating

Ultrathin PET films were grown on the tin nanoparticles by molecular layer deposition in a custom-built atmospheric-pressure fluidised bed reactor, described elsewhere [19], [23]. The MLD precursors, terephthaloyl chloride (TC) and ethylene glycol (EG), were contained within separate stainless steel bubblers under an inert atmosphere, and were heated to 100 °C and 105 °C respectively. The reactor temperature was maintained at 150 °C by an infrared lamp with a feedback control. A MLD cycle consisted of sequential exposures to TC (0.5 min)-N_2 (5 min)-EG (1 min)-N_2 (5 min). In each experiment, ~20 g of Sn nanopowder were loaded into the reactor and fluidised with a flowrate of 1 L min^{-1}. 50 MLD cycles were performed to obtain low-nano PET coatings on the tin nanoparticles.

2.3 Nanofluid production

Nanofluids at 1 mass % (0.137 volume %) were prepared. Surfactant concentration was varied from 0 to 1 ml g^{-1} of thermal oil to determine the optimal value required for a stable nanofluid. The nanofluids were obtained with the following procedure. First, the pure thermal oil was heated to 80 ºC in a hot plate C-MAG HS 7 (IKA Labotechnik). Then, the surfactant (if used) was added, followed by sonication of the mixture for 1 minute using an ultrasound probe (Sonopuls HD2200, Bandelin, HF-output of 200 W and HF-frequency of 20 kHz). Afterwards, the nanoparticles were added and the nanofluid was sonicated a further five minutes. During sonication, the fluid temperature was controlled to not exceed 90 ºC. A total of 9 samples were prepared, combining different nanoparticles and surfactants. Samples are identified by the nanoparticle, the surfactant used and the surfactant concentration as shown in Table 1.

Table 1. Sample identification X-Y-Z

X - - **Nanoparticle**	**- Y –** **Surfactant**	**- - Z** **Surfactant concentration (ml g^{-1} of thermal oil)**
Sn	S0' - No surfactant without sonication	-
	S0 - No surfactant	-
	S1- Oleic acid 90%	0.1
	S2 - Oleic acid 97%	0.1
	S3 – Virgin olive oil	0.1
		0.05
		0.025
		0.005
Sn@PET	S0 - No surfactant	-

3. Experimental techniques

Field Emission Transmission Electron Microscopy, TEM

The morphology and size of the primary nanoparticles, as well as the thickness of the coatings were observed by means of Transmission electron microscopy (TEM) using a JEM 1010 (JEOL) microscope operating at a voltage of 100 kV. Nanoparticles were dispersed in ethanol and a droplet of the fluid was dispersed onto a carbon-coated copper-based TEM grid. The liquid content was then removed by evaporation so the solid particles remained on the grid surface.

The particle size distribution was obtained by image processing of over 600 particles observed in the TEM micrographs. The PET film thickness was measured at multiple locations of the Sn nanoparticles and then averaged.

Fourier-transform Infrared Spectroscopy, FTIR

Chemical composition of the different samples studied were analysed using a FTIR-6200 spectrometer (Jasco) with a spectral window of 2000–600 cm^{-1} in transmission mode. A small amount of sample (~1 wt.%) was mixed with KBr (IR spectroscopy grade, Scharlab SL), grounded and pressed into pellets of 13 mm of diameter.

High Temperature Stability

The colloidal stability of the nanofluids was evaluated by visual observation of the sample before and after a thermal treatment at 140 ºC in an oven for 24h. Images of the samples (in 10ml vials, 23x45mm) were taken to compare the settling of the nanoparticles for the different formulations under study.

Thermogravimetric Analysis, TGA

The thermal stability of the nanofluids and the base fluids was measured by means of thermogravimetric analysis (TGA) (Mettler Toledo). Fluid samples were submitted to a 5 minute isotherm followed by a heating step from 25 ºC to 450 ºC at 10 K min^{-1} under N_2 atmosphere.

Dynamic Light Scattering, DLS

To measure the particle size distribution of the particles or agglomerates suspended in the nanofluid, dynamic light scattering tests were performed using a Zetasizer Nano ZS particle size analyser (Malvern Panalytical). The equipment is composed of a laser, that illuminates the cell containing the sample, and a detector that acquires the intensity of the light scattered by the particles suspended. Both the laser and detector are enclosed in the device, and the hydrodynamic diameter is calculated based on the intensity of the scattered light at 173 º. The stability of the sample with temperature was evaluated by this method, analysing the evolution of the hydrodynamic diameters of the particles and clusters of agglomerated particles with this variable. The tests were performed at room temperature (25 ºC) and the maximum temperature allowed by the equipment (70 ºC) to determine the evolution of the particle size distribution with temperature.

Transient Hot Wire, THW

The thermal conductivity of the samples was measured by means of the transient hot wire technique using a KD2 Pro conductimeter (Decagon Devices Inc.) with an accuracy of ±0.01 W m^{-1} K^{-1} in the 0.02 to 0.2 W m^{-1} K^{-1} range. Taken into account the range of values measured in this research, these values correspond to a maximum of 8.32%. The device has been calibrated following the recommendations of the manufacturer, with a glycerin verification standard before the measurements [24]. In spite of the controversy respect to the use of the KD2 Pro to measure thermal conductivity in nanofluids [25], its use for the thermal oil employed in this work has been previously accepted in the literature [26]–[30] with only one work to the best of the author's knowledge that uses a different technique [31]. Therefore, and given its availability in the facilities of the research group, the decision was to use it, following the conclusion

reached by Buongiorno et al. [32] that despite systematic differences between measurement techniques, as long as the same technique at the same conditions is used to measure the thermal conductivity of the base fluid and the nanofluid, the enhancement is consistent between measurement techniques.

The sample was introduced in a sealed glass tube (20 ml) where the sensor was inserted vertically. To carry out the test at high temperatures, the tube was immersed in a thermostatic bath with controlled temperature. The maximum temperature reached by this equipment is 150 ºC. Measurements were carried out at 80 ºC, 100 ºC, 120 ºC and 140 ºC and a total number of 5 tests were run for each sample in order to obtain a mean value for each temperature. The experimental error, ε, was obtained from the standard deviation, σ, of the n measurement taken:

$$\varepsilon = t_{n-1,0.025}\frac{\sigma}{\sqrt{n}} \qquad (1)$$

where $t_{n-1,0.025}$ is the Student's t-distribution for n-1 degrees of freedom and 95% of confidence level. The average of this experimental error for the thermal conductivity measurements was of 1.81%.

Rheometry

The dynamic viscosity of the samples was obtained by performing tests under steady state conditions using a Discovery HR-1 rheometer (TA Instruments). The minimum and maximum torque of the rheometer are 20 nN·m and 150 nN·m respectively, with a torque resolution of 0.1 nN·m, A system composed of two parallel plates (Diameter = 40 mm) inside an environmental test chamber was used to measure viscosity at 80 ºC, 100 ºC, 120 ºC and 140 ºC. Reliable measurements could not be obtained at higher temperatures due to sample evaporation. Measurements were performed applying a constant shear rate of 100 s^{-1} for two minutes. Samples were kept at the desired conditions for 5 minutes before commencing measurements to ensure temperature stabilisation. The experimental error was statistically obtained at a 95% of confidence level (equation 1), with an average error of 0.59%.

Differential Scanning Calorimetry, DSC

The specific heat of the samples was measured with a differential scanning calorimeter (DSC2, Mettler Toledo) able to reach temperatures up to 700 ºC. The DSC sensor contains 120 thermocouples (AuAuPd) with a resolution of 0.02 μW and temperature accuracy and precision of ±0.2 K and ±0.02 K respectively. The *areas method* was used to study specific heat at 80 ºC, 100 ºC, 120 ºC and 140 ºC twice in a cycle, during the heating and cooling processes. A 1 ºC temperature step was applied at each temperature, with 5

minute isotherms before and after the step. All the specific heat tests were carried out with a constant 25 ml min^{-1} N_2 flow rate. An aluminium crucible (40 µl) was used. Four samples (20 mg) of each nanofluid were prepared and two cycles were run in order to obtain a mean value. The experimental error was statistically obtained at a 95% of confidence level (equation 1), with an average error of 1.07%.

4. Results and discussion

4.1 Nanoparticle characterization

The average diameter of the nanoparticles and their morphology was observed using Transmission Electron Microscopy for both Sn and Sn@PET, as shown in Figure 1. Figure 1 b) also presents the PET coating observed in the Sn@PET nanoparticles, with a value of ~3.7 nm when averaged in multiple locations. This translates into a growth per cycle of ~0.07 nm, in good agreement with the values reported in literature on OH-terminated surfaces [19], [33].

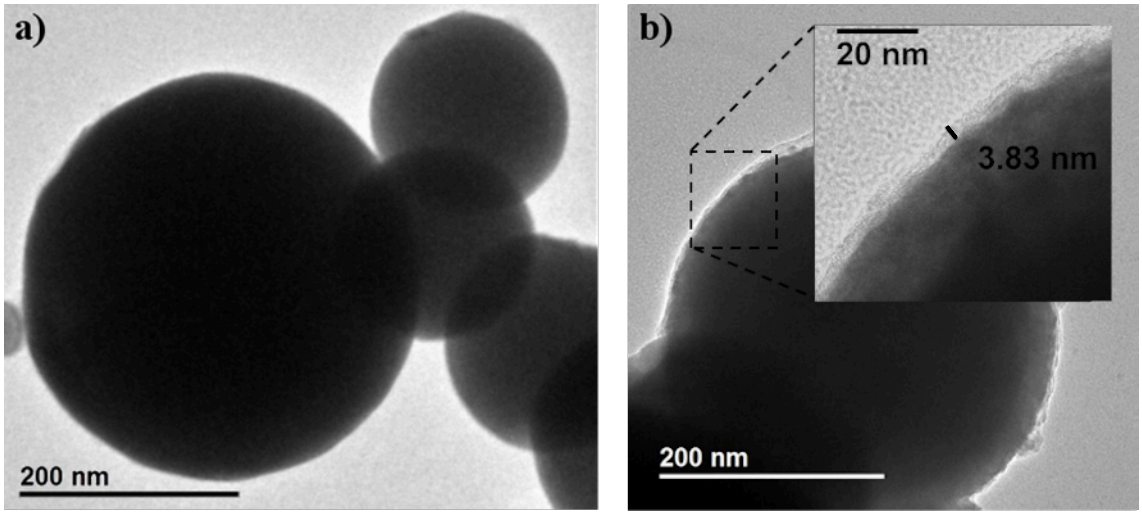

Figure 1. TEM micrographs of a) Sn and b) Sn@PET, including a high magnification detail of the PET coating

The images of more than 600 nanoparticles allowed to create a representative particle size distribution of both materials (Figure 2). The mean diameter obtained by image processing was considering as the average size that presented at least a half of the particles studied (D50). The obtained D50 values for Sn and Sn@PET were essentially identical, further demonstrating that aggregates were not formed during the MLD process.

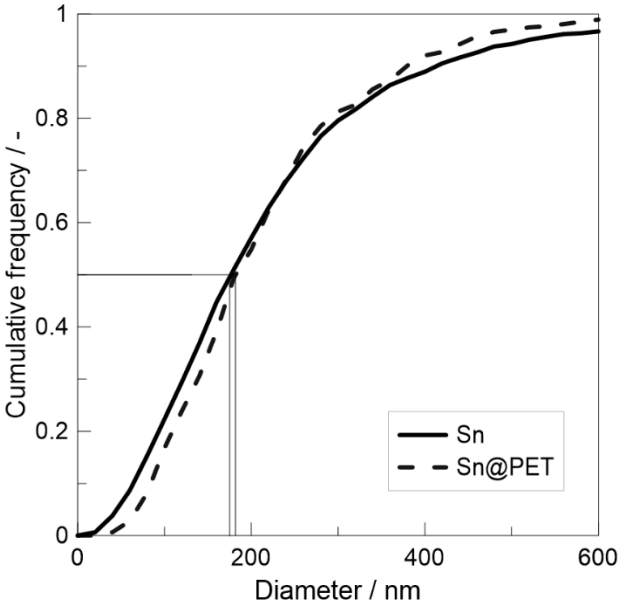

Figure 2. Particle size distribution of the Sn and Sn@PET nanoparticles obtained from TEM images

FTIR spectra (Figure 3) were taken to prove the deposition of PET onto the Sn nanoparticles. The strong band at 1717 cm^{-1}, attributed to the ester carbonyl stretch, is typical of aromatic esters [33]. Several peaks arise from both the ethylene glycol moiety and the benzene ring constituting PET. The glycol group exhibits the CH_2 wagging band at 1340 cm^{-1}, the symmetric C-O stretch at 1099 cm^{-1} and the antisymmetric C-O stretches at 1044 and 971 cm^{-1} [34]–[36]. The phenyl group shows the ring-ester in-plane modes at 1122 and 1255 cm^{-1} as well as in-plane vibrations at 1407 and 1018 cm^{-1}, and out-of-plane deformations at 872 and 727 cm^{-1} [37].

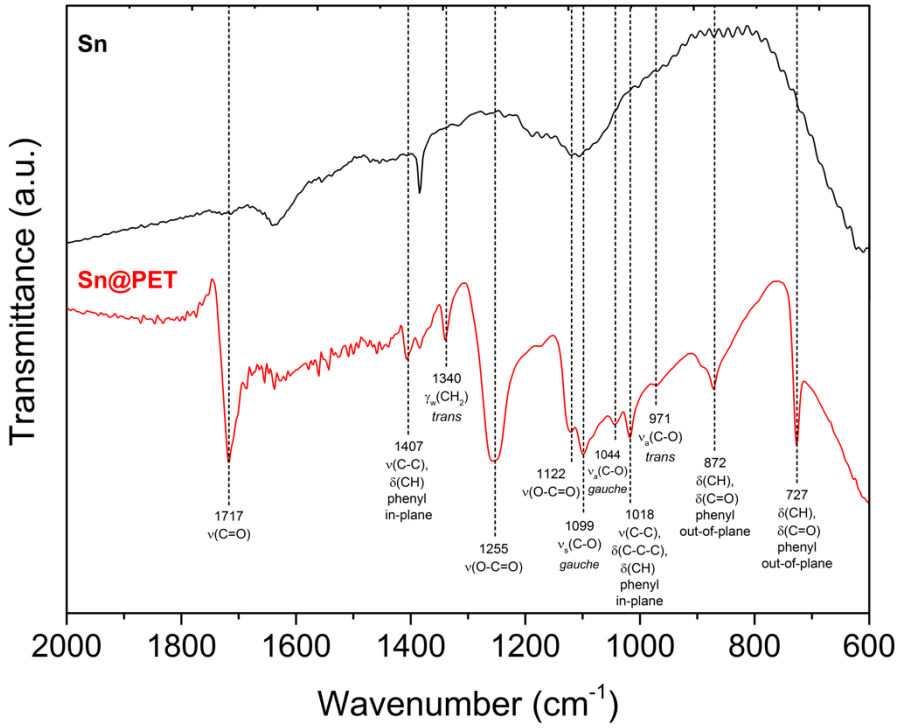

Figure 3. FTIR spectra of the Sn and Sn@PET nanoparticles, including the identification of peaks arising from PET

4.2 Nanofluid stability

Colloidal stability and particle size

The most suitable surfactant in order to stabilise the Sn nanoparticles in the thermal oil, according to the surfactant stabilization approach, was first evaluated. Nanofluids containing oleic acid, a widespread surfactant used to form stable colloidal suspensions, with 90% (S1) and 97% (S2) purity and virgin olive oil (S3) were prepared. The concentration of surfactant for all the samples in the base fluid was 0.1 ml g^{-1}. Figure 4 shows the nanofluids mentioned above after 24 h in an oven at 140 ºC.

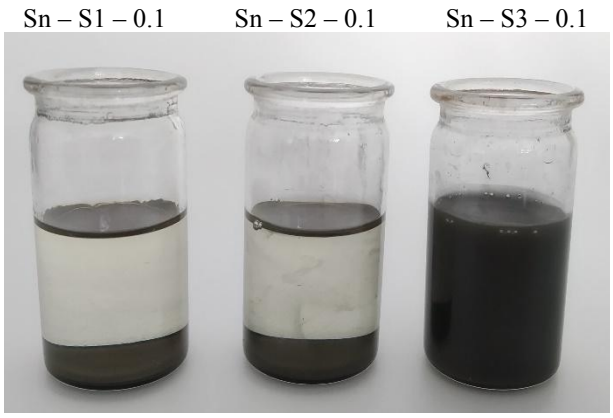

Figure 4. Influence of the surfactant type on the Sn nanofluids stability after 24h at 140ºC (10ml vials)

From the visual examination after 24h, it was evident that both samples with oleic acid were completely unstable, and the nanoparticles settled at the bottom of the vial. However, the sample synthesised with olive oil (Sn – S3 – 0.1) was stable after 24 h at 140 ºC. As a result, olive oil was chosen as surfactant for further tests.

The next step was to determine the optimal concentration of olive oil needed to ensure a good level of nanofluid stability, while minimizing the effect of the surfactant on the base fluid. In order to do this, six samples were prepared: samples S0' (no sonication) and S0, containing no surfactant, and four more samples with concentrations of surfactant of 0.005, 0.025, 0.05 and 0.1 ml g^{-1} of base fluid. The samples were submitted to 24 h in the oven at 140 ºC. The state of the nanofluids after the tests is shown in Figure 5, where the influence of the surfactant concentration can be clearly observed.

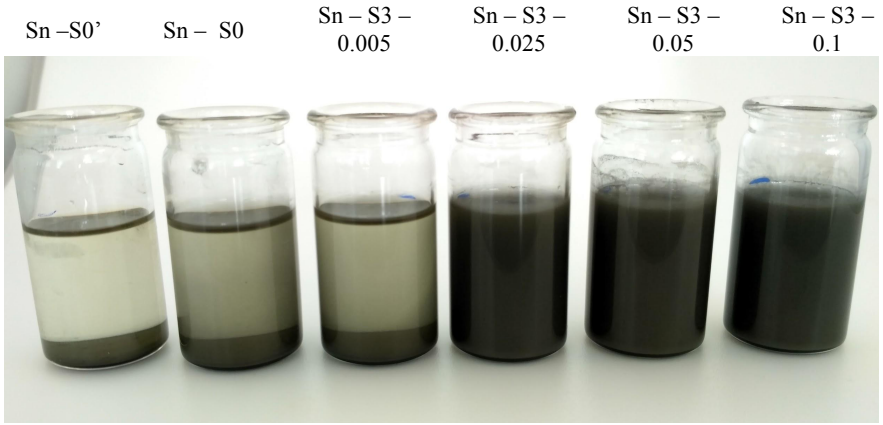

Figure 5. Influence of olive oil concentration on the stability of the Sn nanofluids after 24 h at 140 ºC (increasing olive oil concentration from left to right)

The nanoparticles in both samples with no surfactant (S0, S0`) had sedimented. Sample Sn – S3 – 0.005 had an insufficient concentration of olive oil and was not stable. Samples with virgin olive oil concentrations from 0.025 ml g^{-1} were all stable, and no visual difference could be found between them. On this basis, sample Sn – S3 – 0.025, with a surfactant concentration of 0.025 ml g^{-1}, was selected for further analysis and characterization. This was the sample with the lowest surfactant concentration that could still be used to obtain a stable nanofluid with Sn nanoparticles.

The same stability test was also performed on the nanofluid obtained using the nanoparticles coated with PET (Sn@PET – S0). The PET coating acts as a stabiliser and removes the need for surfactants. Figure 6 shows the comparison of the behaviour of both nanofluids (Sn – S3 – 0.025 and Sn@PET – S0) with respect

to Sn – S0 after 24 h in the oven at 140 ºC. No visual differences were observed and therefore it was concluded that both samples were stable.

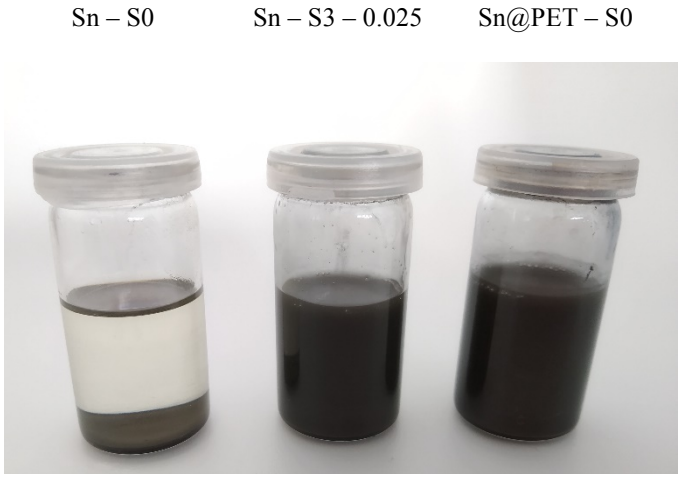

Figure 6. Comparison of Sn -S0 (left), Sn – S3 – 0.025 (center) and Sn@PET – S0 (right) nanofluids stability after 24 h at 140 ºC

The particle size distribution of both stable nanofluids was measured by means of DLS tests. This technique helped determine the level of agglomeration of the dispersed nanoparticles at room temperature (25 ºC) and the influence of the temperature on the particle agglomeration when heated at 70 ºC. The particle size distributions obtained for the nanofluids are plotted in Figure 7. From the distributions, the mean particle size within the nanofluid, D50, was obtained and results are shown in Table 2.

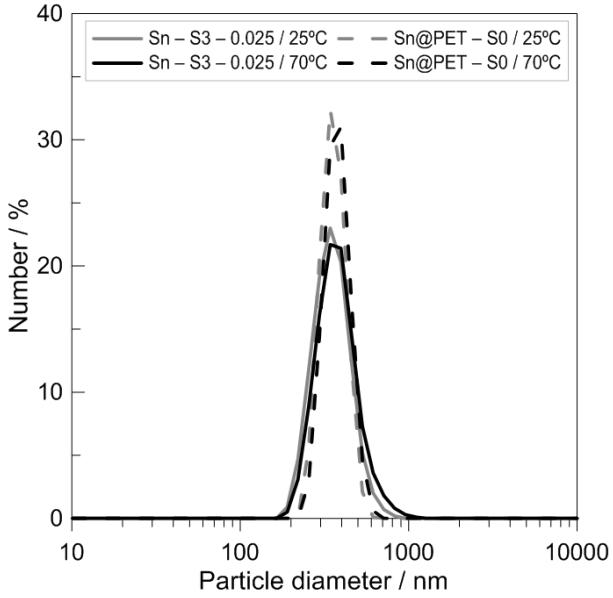

Figure 7. Particle size distribution within the nanofluids at 25 ºC and 70 ºC obtained from DLS

Table 2. Mean particle size for nanoparticles within nanofluids at 25 ºC and 70 ºC.

	Mean particle size, D50 / nm	
Temperature / ºC	**Sn – S3 – 0.025**	**Sn@PET – S0**
25	346.33	330.67
70	356.67	376.83

No significant differences were obtained for the particle size distributions and the mean diameters for both nanofluids (Sn – S3 – 0.025 and Sn@PET – S0). However, compared to TEM sizes in Figure 2, the results indicate that the nanoparticles agglomerate to a small degree when they are suspended in the base fluid, as both present bigger particle sizes than the primary nanoparticles measured by TEM.

Regarding the influence of temperature, the mean particle size slightly increases for both samples but the differences found in the particle size distributions are negligible. These results confirm the stability of both samples at temperature conditions up to 70 ºC.

Thermal stability

The thermogravimetric analysis (TGA) was performed submitting the samples to temperatures from 25 ºC to 450 ºC to give information about the maximum working temperatures of the studied samples: two base fluids (pure TH66 and mixture of TH66 and olive oil) and two stable nanofluids (Sn – S3 – 0.025 and Sn@PET – S0). The initial decomposition temperature (IDT) or onset, which corresponds to the maximum temperature that the fluids could withstand before starting degradation, was established as the temperature at which a 1.5% of mass loss is observed. The maximum rate of decomposition temperature (MRDT), i.e. the point where the maximum quantity of the sample is being degraded, was also obtained. Figure 8 shows the TGA curves measured from which the decomposition temperatures in Table 3 are obtained.

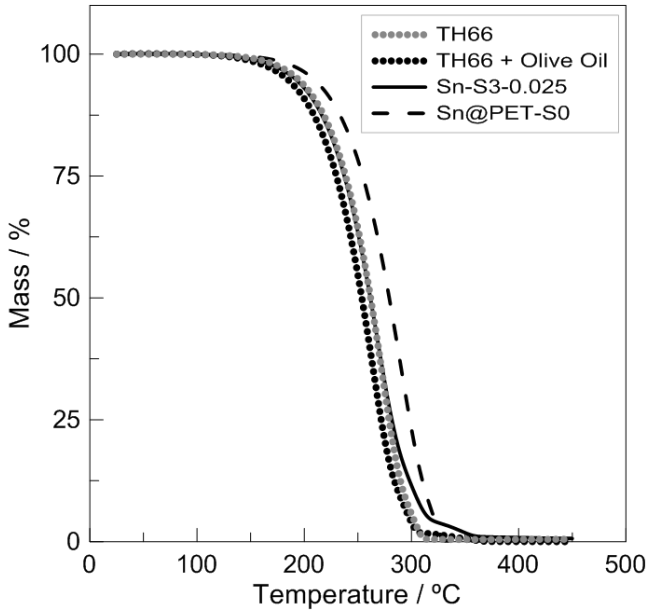

Figure 8. Thermal stability (TGA curves) of two base fluids and two stable nanofluids

Table 3. Initial decomposition and maximum rate of decomposition temperatures, determined by TGA

Sample	Initial decomposition temperature (IDT) / ºC	Maximum rate of decomposition temperature (MRDT) / ºC
TH66	164.4	273.8
TH66 + Olive oil	154.6	267.9
Sn – S3 - 0.025	162.5	272.5
Sn@PET - S0	176.9	290.5

The results indicate that the addition of the olive oil as surfactant decreases the working temperature of the Therminol 66. However, the addition of the nanoparticles leads to an increase in both IDT and MRDT temperatures and the initial values for pure Therminol 66 are recovered for Sn-S3-0.025. Furthermore, where no surfactant is used with the coated nanoparticles (Sn@PET-S0), the IDT and MRDT of the base HTF are improved. It can be concluded that the use of nanofluids does not affect significantly to the maximum working temperatures and that nanofluids can be used as a substitute of Therminol 66 in high temperature applications.

4.3 Nanofluid characterization

For the two stable nanofluids produced, Sn – S3 – 0.025 and Sn@PET – S0, thermal conductivity, viscosity and specific heat were experimentally measured to evaluate the effect of the nanoparticles and their potential as heat transfer fluids. The accuracy of the measurements was determined by comparing the

experimental results with theoretical values provided by the manufacturer or calculated using existing theoretical models available in literature. The comparison between the measured and theoretical values could be useful to identify possible systematic errors in the measurements of certain variables, especially in the case of Therminol 66 values, as they do not involve further equations and data. However, both base fluids and nanofluids are measured with the same equipment, so the experimental ratios between those two samples are expected to be consistent [32].

The relative error, ε_r, between theoretical, *th*, and experimental, *exp*, results was calculated for all the properties as follow:

$$\varepsilon_r = \frac{|th - \exp|}{th} \cdot 100 \qquad (2)$$

For the calculations, tin properties were obtained from [38] while the olive oil properties were taken from the literature [39]–[41]. Theoretical values for pure Therminol 66 were taken from the manufacturer data sheet [42]. These data are based in samples tested in the laboratory and not guaranteed for all samples by the manufacturer. However, the data are used in this study as reference for the experimental data, as to the best of the authors knowledge, there are no other systematic data of those thermal properties at the measured temperatures.

The error bars in the figures of the thermal properties ratios were calculated using error propagation equation and the experimental errors defined in Section 3.

Thermal conductivity, *k*

Thermal conductivity is the most important parameter to define the heat transfer properties of a fluid. Experimental results for the four samples measured (base fluids and nanofluids) are shown in Table 4.

The mixture rule was used to calculate the thermal conductivity of the Therminol 66 and olive oil sample. The thermal conductivity of the nanofluids was calculated using the equation for the effective conductivity of Maxwell's model [43]:

$$k_{nf} = \frac{k_{np} + 2k_{bf} + 2(k_{np} - k_{bf})\phi}{k_{np} + 2k_{bf} - (k_{np} - k_{bf})\phi} k_{bf} \qquad (3)$$

where ϕ is the volume fraction of nanoparticles and k_{nf}, k_{np} and k_{bf} are the thermal conductivities of the nanofluid, nanoparticle and base fluid, respectively.

It can be observed that the experimental values obtained for all the fluids were higher than the theoretical values expected, and also that this difference increases with temperature. Previous investigations have also reported that the thermal conductivity of nanofluids with metallic nanoparticles is underpredicted by Maxwell theory [29], [44].

Table 4. Thermal conductivity results

	Temperature / ºC	**Experimental *k* / W m^{-1} K^{-1}**	**Theoretical *k* / W m^{-1} K^{-1}**	**Error / %**
TH66	80	0.1236	0.1147	7.76
	100	0.1222	0.1135	7.67
	120	0.1212	0.1121	8.12
	140	0.1202	0.1107	8.58
TH66 + Olive oil	80	0.1272	0.1157	9.91
	100	0.1284	0.1143	12.34
	120	0.1250	0.1131	10.48
	140	0.1234	0.1117	10.47
Sn – S3 - 0.025	80	0.1266	0.1162	8.95
	100	0.1252	0.1150	8.87
	120	0.1271	0.1136	11.88
	140	0.1312	0.1122	16.93
Sn@PET - S0	80	0.1274	0.1152	10.62
	100	0.1284	0.1140	12.67
	120	0.1290	0.1126	14.61
	140	0.1277	0.1112	14.89

The experimental thermal conductivity ratios for both nanofluids with respect to their base fluids are plotted in Figure 9. It can be observed that it increases with temperature and a maximum enhancement of 9.1% and 6.6% was achieved for Sn – S3 – 0.025 and Sn@PET – S0 respectively when compared to pure TH66.

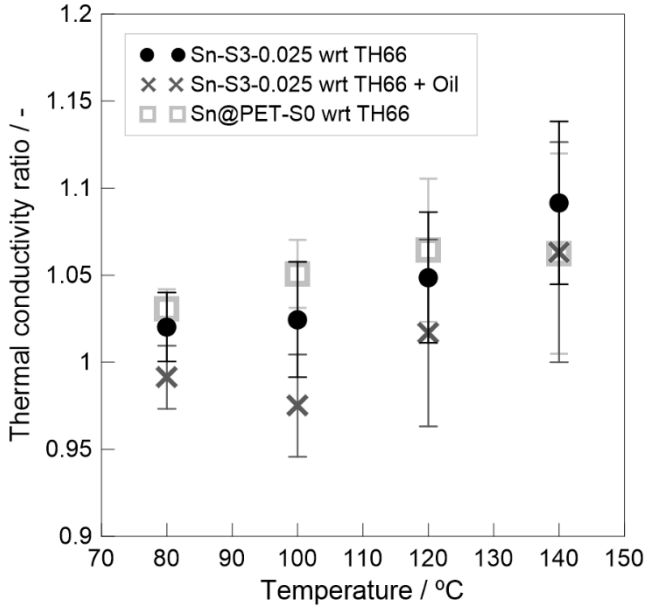

Figure 9. Nanofluids with respect to base fluids experimental thermal conductivity ratios

Dynamic viscosity, η

The dynamic viscosity is directly related with the flow and heat transfer properties of the fluids. In order to compare the different samples, measurements at a constant shear rate of 100 s^{-1} were taken. The Newtonian behaviour was observed in a previous work [45] for pure Therminol 66 and the shear rate was checked to do not exceed the maximum value from which turbulence effects appear. Experimental results for the four samples measured (base fluids and nanofluids) are shown in Table 5. The nanofluid viscosity was calculated using Einstein's equation:

$$\eta_{nf} = \eta_{bf}(1 + 2.5\phi) \qquad (4)$$

where ϕ is the volume fraction of nanoparticles and η_{nf} and η_{bf} are the viscosities of the nanofluid and base fluid respectively.

In the results presented in Table 5, it can be observed that the viscosity decreases with temperature as expected. The error between experimental and theoretical values is lower than 13% for all the measurements. The nanofluid viscosities obtained with Einstein's equation are in good agreement with the experimental values.

Table 5. Viscosity results

Temperature / ºC	**Experimental η / Pa s**	**Theoretical η / Pa s**	**Error / %**	**Temperature / ºC**
TH66	80	0.00523	0.00593	11.84
	100	0.00318	0.00361	11.50
	120	0.00215	0.00242	10.93
	140	0.00158	0.00175	9.66
TH66 + Olive oil	80	0.00528	0.00605	12.70
	100	0.00325	0.00368	11.69
	120	0.00226	0.00248	8.93
	140	0.00166	0.00179	7.33
Sn – S3 - 0.025	80	0.00530	0.00607	12.61
	100	0.00331	0.00369	10.37
	120	0.00230	0.00249	7.49
	140	0.00172	0.00180	4.46
Sn@PET - S0	80	0.00553	0.00595	7.11
	100	0.00330	0.00361	8.64
	120	0.00223	0.00243	8.03
	140	0.00162	0.00175	7.71

The experimental viscosity ratios for both nanofluids are plotted in Figure 10. Considering the gathered experimental data, a gradual increase in the viscosity ratio of the nanofluid Sn – S3 – 0.025 with temperature compared to pure TH66 can be observed. This leads to a viscosity increment of 8.8% at 140 ºC. In this case, both the nanoparticles and the oil contribute to the viscosity increment, Considering only the impact of Sn nanoparticles on the viscosity, the increase is of only 3.4% at 140 ºC, comparing the values of this nanofluid with the TH66 and oil mixture. This increment is almost constant with temperature and possible differences lay within the experimental error. Regarding the Sn@PET – S0 nanofluid, in which no additives are present and only the impact of coated Sn nanoparticles is observed, the viscosity increment can be also considered constant with temperature at around 3%. The higher increment observed for the lowest temperature lay also within the experimental error. It can be concluded that the influence of the temperature on the viscosity increment is almost negligible when only the effect of the nanoparticles is taken into account and the viscosity of the nanofluids are compared with respect to their own base fluids (TH66 and oil mixture for Sn-S3-0.25 and pure TH66 for Sn@PET-S0)..

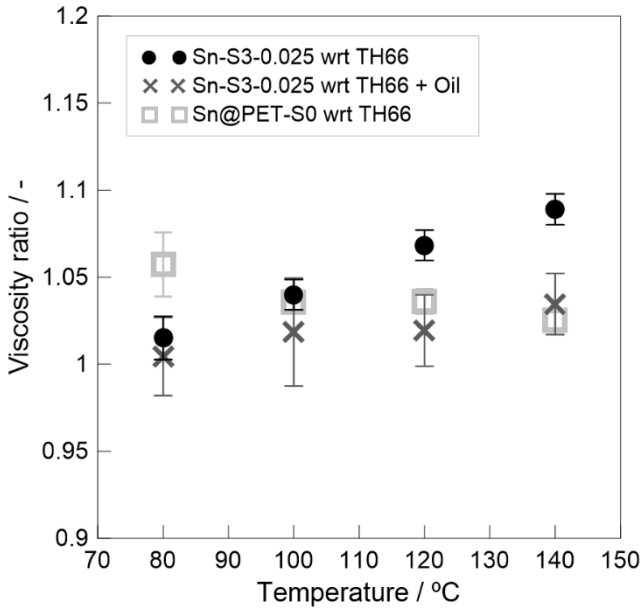

Figure 10. Nanofluids with respect to base fluids experimental viscosity ratios

Specific heat capacity, c_P

Experimental results for the four measured samples are shown in Table 6. The mixture rule was used to calculate the specific heat of the Therminol 66 and olive oil sample. Specific heat of the nanofluids was also calculated by means of the mixture rule:

$$c_{P,nf} = w \cdot c_{P,np} + (1 - w) \cdot c_{P,bf} \qquad (5)$$

where w is the solid mass fraction, $c_{p,nf}$, $c_{p,np}$ and $c_{p,bf}$ are the specific heat values of the nanofluid, nanoparticle and base fluid respectively.

The samples were tested experimentally using the DSC from 80 ºC to 140 ºC to obtain the specific heat. The results indicate that the mixture rule can be used to predict the specific heat of the samples with a lower than 2.5% difference between experimental data and theoretical values.

Table 6. Specific heat results

	Temperature / ºC	**Experimental c_P / J g^{-1} K^{-1}**	**Theoretical c_P / J g^{-1} K^{-1}**	**Error / %**
TH66	80	1.782	1.768	0.79
	100	1.856	1.837	1.03
	120	1.921	1.908	0.68
	140	1.997	1.978	0.96
TH66 + Olive oil	80	1.805	1.768	2.09
	100	1.875	1.836	2.12
	120	1.935	1.906	1.52
	140	2.007	1.974	1.67
Sn – S3 - 0.025	80	1.781	1.752	1.66
	100	1.858	1.819	2.14
	120	1.927	1.888	2.07
	140	1.99	1.955	1.79
Sn@PET - S0	80	1.745	1.752	0.40
	100	1.828	1.82	0.44
	120	1.893	1.89	0.16
	140	1.968	1.959	0.46

The experimental specific heat ratios are plotted in Figure 11. The addition of tin nanoparticles with lower specific heat than the base fluid should have a negative effect in the specific heat. The ratios obtained for both nanofluids indicate a slight reduction of the specific heat as expected from the mixture rule calculations, obtaining experimental errors lower than 2%. For the uncoated tin nanoparticles the decrease in the specific heat with respect to Therminol 66 is negligible while it becomes slightly more noticeable for the Sn@PET nanoparticles.

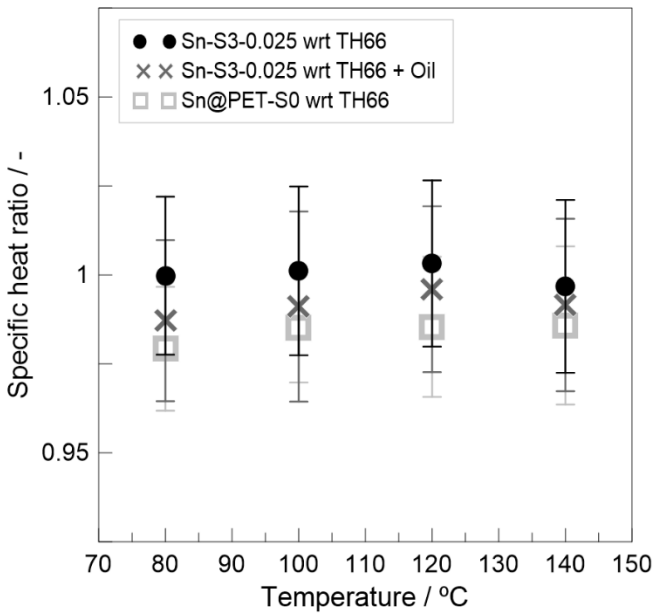

Figure 11. Nanofluids with respect to base fluids experimental specific heat ratios

Prandtl number, Pr

The results of the three physical properties measured can be used to obtain directly the Prandtl number, which can be calculated both for the base fluids and the nanofluids according to the following equation:

$$Pr = \frac{c_p \eta}{k} \qquad (6)$$

The low variation in the specific heat between all the fluids implies that the Prandtl number will approximately describe the viscosity with respect to the thermal conductivity. Due to this reason, lower Prandtl number reflect that a better thermal performance can be achieved with lower viscosities, meaning less power used to pump the fluids.

As a result of these calculations the behaviour of the Prandtl number can be predicted at different temperatures, which are showed in Table 7 along with the error between the expected theoretical values and the results using the experimental measurements.

Table 7. Prandtl number results

	Temperature / ºC	**Experimental Pr / -**	**Theoretical Pr / -**	**Error / %**
TH66	80	75.37	91.41	17.54
	100	48.47	58.27	16.82
	120	34.21	41.19	16.93
	140	26.31	31.27	15.87
TH66 + Olive oil	80	74.96	92.45	18.92
	100	47.50	59.18	19.74
	120	34.96	41.79	16.34
	140	27.07	31.74	14.70
Sn – S3 - 0.025	80	74.68	91.56	18.44
	100	49.17	58.47	15.91
	120	34.90	41.37	15.63
	140	26.13	31.40	16.79
Sn@PET - S0	80	75.71	90.52	16.36
	100	46.99	57.69	18.55
	120	32.77	40.77	19.64
	140	24.98	30.95	19.28

The combination of the divergences between theoretical and experimental results for the three properties lead to errors included between 15 and 20%. The comparison between the Prandtl of the nanofluids and their respective base fluids has been reflected in Figure 12.

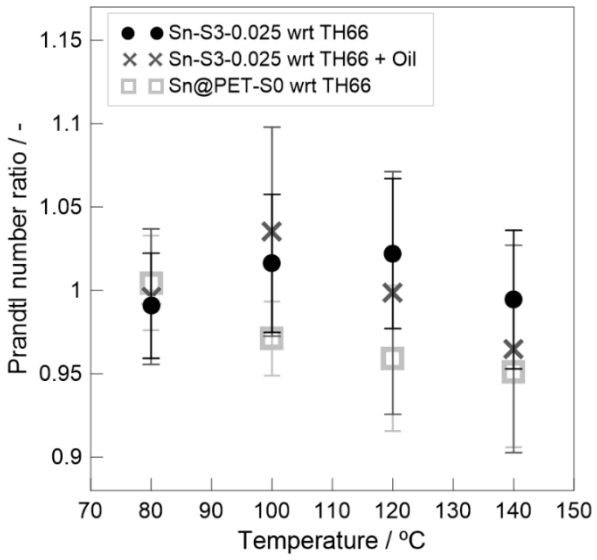

Figure 12. Evolution of Prandtl number ratio with temperature

Two different trends are observed in the figure. For the Sn-S3-0.25 samples the Prandtl number ratio increases with temperature up to a maximum value and then a decrease is achieved. This behaviour can be related to the evolution of their thermal conductivity and viscosity with temperature. In these samples the thermal conductivity remains initially constant while the viscosity ratio increases. However, from 100ºC their thermal conductivity increases thus compensating the increase in the viscosity. For the Sn@PET-S0 a continuous decrease is observed. In this case, as the viscosity can be considered almost constant with temperature the evolution of the Prandtl number ratio is directly affected by the thermal conductivity ratio. The continuous increase with temperature obtained for this property leads to a decrease in the Prandtl number. As a result, in all the samples a reduction of the Prandtl number with respect to the corresponding base fluids can be achieved corroborating the suitability of the nanofluids for heat transfer applications.

Heat transfer coefficient, *h*

Once the thermophysical properties of the stable nanofluids were experimentally measured, their potential use in heat transfer applications was evaluated through the calculation of the heat transfer coefficient, following the guidelines for nanofluids described in [12]. The ratio between the nanofluid and the base fluid was obtained with the experimental values of thermal conductivity, dynamic viscosity and specific heat capacity previously measured.

The heat transfer coefficient can be calculated from the Nusselt number, *Nu*:

$$Nu = \frac{h \cdot D}{k} \qquad (7)$$

where *D* is a geometry factor characteristic of the test section.

For a laminar flow regime, the Nusselt number is considered to be constant in the fully developed region (*Nu* = 3.66 for circular pipes) and thus the increase in the heat transfer coefficient equals the thermal conductivity enhancement. However, for turbulent flow regime the Nusselt number depends on the Reynolds, *Re,* and Prandtl, *Pr,* numbers which depend in turn on the thermal conductivity, specific heat and viscosity. From the correlations available in the literature, the Gnielinski correlation was proved to better predict the heat transfer coefficient in nanofluids [46]:

$$Nu = \frac{f}{8} \frac{(Re-1000)Pr}{1+12.7\sqrt{\frac{f}{8}}\left(Pr^{\frac{2}{3}}-1\right)} \qquad (8)$$

where *f* is the friction factor calculated by using the Colebrook–White equation:

$$\frac{1}{\sqrt{f}} = -2\log\left[\frac{\varepsilon/D}{3.7} + \frac{2.51}{\mathrm{Re}\sqrt{f}}\right] \qquad (9)$$

where ε is the wall roughness of the pipe. For the calculations a stainless steel pipe with a roughness of 1.5 μm and an inner diameter of 7 mm was considered.

Figure 13 shows the heat transfer ratios between the nanofluids and the corresponding base fluids at 80 ºC and 140 ºC for both laminar and turbulent flow regime, on a constant Reynolds basis. The experimental data obtained for thermal conductivity, viscosity and specific heat showed that for laminar flows the improvement achieved at 140 ºC was about 9.3% for the Sn – S3 – 0.025 nanofluid and 6.4% for Sn@PET–S0 compared to TH66 as base fluid.

In turbulent flows, the heat transfer ratio can be considered constant with the Reynolds number and a 9% enhancement at 140 ºC can be achieved for the Sn – S3 – 0.025 nanofluid. For the Sn@PET – S0 nanofluid, the enhancement is lower due to the difference in the thermophysical properties such as the lower specific heat of the mixture. For this nanofluid a maximum enhancement of 4.5% at 140 ºC is predicted. At 80 ºC both Sn@PET – S0 and Sn – S3 – 0.025 present quite similar results within the experimental errors. For both nanofluids and flow regimes, there is an increasing trend of the heat transfer coefficient ratio with temperature up to 140 ºC. For higher temperatures, this trend can only be experimentally confirmed with equipment which can operate at higher temperatures or high temperature heat transfer loops.

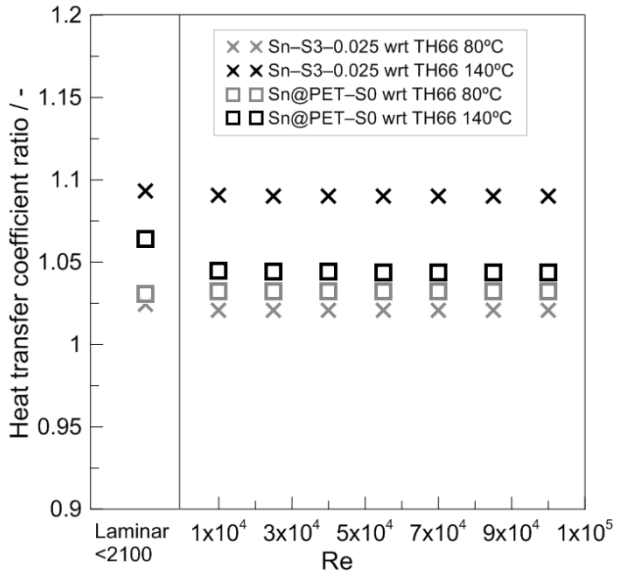

Figure 13. Evolution of heat transfer ratio with temperature and Reynolds number

5. Conclusions

Tin nanoparticles were stabilised in Therminol 66 to produce a nanofluid with enhanced properties for use in heat transfer applications. Two different methods were evaluated to obtain a stable suspension. In the first approach, the suitability of different surfactants was tested. Oleic acid, commonly used in the literature, was unable to stabilise the nanoparticles, whereas the virgin olive oil biosurfactant was suitable to produce stable nanofluids. In the second approach, nanoscale PET films were grown on the tin nanoparticles by MLD, enhancing their dispersibility within the thermal oil. Both nanofluids (Sn – S3 – 0.025 and Sn@PET – S0) demonstrated good stability after treatment for 24 h in an oven at 140 ºC.

Thermophysical properties of both nanofluids were experimentally measured at temperature conditions up to 140 ºC:

- A similar enhancement in thermal conductivity, which also increases with temperature, was achieved for both nanofluids. As previously observed in the literature for metallic nanoparticles, the experimental results are higher than the values predicted by the Maxwell model.
- Both nanofluids present a similar constant increase in the viscosity when compared to their own based fluids. However, if the Sn – S3 – 0.025 nanofluid is compared to the pure Therminol 66 the viscosity ratio is higher and increases with temperature due to the effect of the surfactant. The experimental values can be predicted by the Einstein's equation.
- The specific heat decreases as expected from the mixture rule, but the decrease is negligible for the Sn-S3-0.025 nanofluid with respect to pure Therminol 66. Differences between the experimental and theoretical values are lower than 2.5%.

The heat transfer performance of the nanofluids was evaluated using the experimental results obtained for the thermophysical properties. In laminar flow regime the heat transfer coefficient ratio equals the thermal conductivity ratio and an enhancement of 9.3% and of 6.4% can be achieved at 140 ºC for the Sn – S3 – 0.025 and Sn@PET–S0 respectively. In turbulent flow regime, the enhancement for the Sn – S3 – 0.025 nanofluid (9%) is higher than for the Sn@PET-S0 nanofluid (4.5%). In order to confirm the experimental trend of higher heat transfer ratios observed from 80 ºC to 140 ºC, experiments with either thermo-physical measuring equipment or loops working beyond that value are required.

On the basis of the results presented in this work, the nanofluid stabilised by means of the olive oil biosurfactant is promising for heat transfer applications. Furthermore, the addition of the olive oil biosurfactant is more straightforward than the alternative MLD route investigated, allowing a higher

nanofluid production rate. Nonetheless, the controlled growth of PET film thickness provided by MLD enables the PET content of the coated tin nanoparticles to be fine-tuned, which may lead to enhanced nanofluid properties.

Acknowledgments

The authors want to thank the financial support from Universitat Jaume I (project UJI-B2016-47) and Ministerio de Economía y Competitividad (MINECO) (project ENE2016-77694-R). Nuria Navarrete thanks Universitat Jaume I for a pre-doctoral fellowship (Ref. PREDOC/2016/28) and a research mobility grant (Ref. E-2018-10). Authors thank Servicios Centrales de Instrumentacion Científica (SCIC) of Universitat Jaume I for the use of TEM (Maria del Carmen Peiró), TGA and DSC (Cristina Zahonero). This work has been developed by participants of the COST Action CA15119 Overcoming Barriers to Nanofluids Market Uptake (NANOUPTAKE).

References

[1] N. Sezer, M. A. Atieh, and M. Koç, "A comprehensive review on synthesis, stability, thermophysical properties, and characterization of nanofluids," *Powder Technol.*, vol. 344, pp. 404–431, Feb. 2019.

[2] M. H. Ahmadi, A. Mirlohi, M. Alhuyi Nazari, and R. Ghasempour, "A review of thermal conductivity of various nanofluids," *J. Mol. Liq.*, vol. 265, pp. 181–188, Sep. 2018.

[3] S. P. Jang and S. U. S. Choi, "Cooling performance of a microchannel heat sink with nanofluids," *Appl. Therm. Eng.*, vol. 26, no. 17–18, pp. 2457–2463, Dec. 2006.

[4] R. Chein and G. Huang, "Analysis of microchannel heat sink performance using nanofluids," *Appl. Therm. Eng.*, vol. 25, no. 17–18, pp. 3104–3114, 2005.

[5] A. Ijam and R. Saidur, "Nanofluid as a coolant for electronic devices (cooling of electronic devices)," *Appl. Therm. Eng.*, vol. 32, no. 1, pp. 76–82, 2012.

[6] M. Rafati, A. A. Hamidi, and M. Shariati Niaser, "Application of nanofluids in computer cooling systems (heat transfer performance of nanofluids)," *Appl. Therm. Eng.*, vol. 45–46, pp. 9–14,

2012.

[7] Y. H. Lin, S. W. Kang, and H. L. Chen, “Effect of silver nano-fluid on pulsating heat pipe thermal performance,” *Appl. Therm. Eng.*, vol. 28, no. 11–12, pp. 1312–1317, 2008.

[8] Q. He, S. Zeng, and S. Wang, “Experimental investigation on the efficiency of flat-plate solar collectors with nanofluids,” *Appl. Therm. Eng.*, vol. 88, pp. 165–171, 2014.

[9] U. Nithiyanantham, L. González-Fernández, Y. Grosu, A. Zaki, J. M. Igartua, and A. Faik, “Shape effect of Al2O3 nanoparticles on the thermophysical properties and viscosity of molten salt nanofluids for TES application at CSP plants,” *Appl. Therm. Eng.*, vol. 169, no. March 2019, p. 114942, 2020.

[10] S. M. S. Murshed, K. C. Leong, and C. Yang, “Thermophysical and electrokinetic properties of nanofluids - A critical review,” *Appl. Therm. Eng.*, vol. 28, no. 17–18, pp. 2109–2125, 2008.

[11] J. Akhter, S. I. Gilani, H. H. Al-kayiem, M. Ali, and F. Masood, “Characterization and stability analysis of oil-based copper oxide nanofluids for medium temperature solar collectors,” *Materwiss. Werksttech.*, vol. 50, no. 3, pp. 311–319, 2019.

[12] M. H. Buschmann *et al.*, “Correct interpretation of nanofluid convective heat transfer,” *Int. J. Therm. Sci.*, vol. 129, no. June 2017, pp. 504–531, 2018.

[13] G. Colangelo, E. Favale, P. Miglietta, M. Milanese, and A. de Risi, “Thermal conductivity, viscosity and stability of Al2O3-diathermic oil nanofluids for solar energy systems,” *Energy*, vol. 95, pp. 124–136, Jan. 2016.

[14] S. Manikandan and K. S. Rajan, “MgO-Therminol 55 nanofluids for efficient energy management: Analysis of transient heat transfer performance,” *Energy*, vol. 88, pp. 408–416, Aug. 2015.

[15] M. Muraleedharan, H. Singh, S. Suresh, and M. Udayakumar, “Directly absorbing Therminol-Al2O3 nano heat transfer fluid for linear solar concentrating collectors,” *Sol. Energy*, vol. 137, pp. 134–142, Nov. 2016.

[16] N. Yandrapalli, D. Anandan, S. K S, and R. K.s, “High-Temperature Thermo-Physical Properties of Novel CuO-Therminol (R) 55 Nanofluids,” *Nanosci. Nanotechnol. Lett.*, vol. 4, pp. 1209–

1213, Jan. 2012.

[17] S. Akbari, N. H. Abdurahman, R. M. Yunus, F. Fayaz, and O. R. Alara, “Biosurfactants—a new frontier for social and environmental safety: a mini review,” *Biotechnol. Res. Innov.*, vol. 2, no. 1, pp. 81–90, Jan. 2018.

[18] H. Van Bui, F. Grillo, and J. R. Van Ommen, “Atomic and molecular layer deposition: off the beaten track,” *Chem. Commun.*, vol. 53, no. 1, pp. 45–71, 2017.

[19] D. La Zara *et al.*, “Subnano Surface Engineering of TiO 2 Nanoparticles by PET Molecular Layer Deposition : Tuning Photoactivity and Dispersibility,” 2019.

[20] X. Meng, “An overview of molecular layer deposition for organic and organic–inorganic hybrid materials: mechanisms{,} growth characteristics{,} and promising applications,” *J. Mater. Chem. A*, vol. 5, no. 35, pp. 18326–18378, 2017.

[21] N. Navarrete *et al.*, “Nanofluid based on self-nanoencapsulated metal/metal alloys phase change materials with tuneable crystallisation temperature,” *Sci. Rep.*, vol. 7, no. 1, pp. 1–10, 2017.

[22] G. P. García-Inza, A. J. Hall, and M. C. Rousseaux, “Proportion of oleic acid in olive oil as influenced by the dimensions of the daily temperature oscillation,” *Sci. Hortic. (Amsterdam).*, vol. 227, pp. 305–312, Jan. 2018.

[23] N. Navarrete *et al.*, “Improved thermal energy storage of nanoencapsulated phase change materials by atomic layer deposition,” *Sol. Energy Mater. Sol. Cells*, 2019.

[24] Decagon, “Manual KD2 Pro.” .

[25] G. Tertsinidou, M. J. Assael, and W. A. Wakeham, “The apparent thermal conductivity of liquids containing solid particles of nanometer dimensions: A critique,” *Int. J. Thermophys.*, vol. 36, no. 7, pp. 1367–1395, 2015.

[26] E. V. Timofeeva, M. R. Moravek, and D. Singh, “Improving the heat transfer efficiency of synthetic oil with silica nanoparticles,” *J. Colloid Interface Sci.*, vol. 364, no. 1, pp. 71–79, 2011.

[27] M. M. Sarafraz *et al.*, “Assessment of iron oxide (III)–therminol 66 nanofluid as a novel working fluid in a convective radiator heating system for buildings,” *Energies*, vol. 12, no. 22, 2019.

[28] A. Safaei, A. Hossein Nezhad, and A. Rashidi, “High temperature nanofluids based on therminol 66 for improving the heat exchangers power in gas refineries,” *Appl. Therm. Eng.*, vol. 170, no. July 2019, 2020.

[29] D. Singh *et al.*, “Use of metallic nanoparticles to improve the thermophysical properties of organic heat transfer fluids used in concentrated solar power,” *Sol. Energy*, vol. 105, pp. 468–478, Jul. 2014.

[30] S. Cingarapu, D. Singh, E. V. Timofeeva, and M. R. Moravek, “Nanofluids with encapsulated tin nanoparticles for advanced heat transfer and thermal energy storage,” *Int. J. energy Res.*, vol. 38, no. August 2014, pp. 51–59, 2014.

[31] S. Mossaz *et al.*, “Experimental study on the influence of nanoparticle PCM slurry for high temperature on convective heat transfer and energetic performance in a circular tube under imposed heat flux,” *Appl. Therm. Eng.*, vol. 81, pp. 388–398, 2015.

[32] J. Buongiorno *et al.*, “A benchmark study on the thermal conductivity of nanofluids,” *J. Appl. Phys.*, vol. 106, no. 9, p. 094312, Nov. 2009.

[33] T. Ivanova, P. Maydannik, and D. Cameron, “Molecular layer deposition of polyethylene terephthalate thin films,” *J. Vac. Sci. Technol. a*, vol. 30, Jan. 2012.

[34] C. Y. Liang and S. Krimm, “Infrared spectra of high polymers: Part IX. Polyethylene terephthalate,” *J. Mol. Spectrosc.*, vol. 3, no. 1–6, pp. 554–574, Jan. 1959.

[35] W. W. Daniels and R. E. Kitson, “Infrared spectroscopy of polyethylene terephthalate,” *J. Polym. Sci.*, vol. 33, no. 126, pp. 161–170, 1958.

[36] F. J. Boerio, S. K. Bahl, and G. E. McGraw, “Vibrational analysis of polyethylene terephthalate and its deuterated derivatives,” *J. Polym. Sci. Polym. Phys. Ed.*, vol. 14, no. 6, pp. 1029–1046, 1976.

[37] K. C. Cole, A. Ajji, and É. Pellerin, “New Insights into the Development of Ordered Structure in Poly(ethylene terephthalate). 1. Results from External Reflection Infrared Spectroscopy,” *Macromolecules*, vol. 35, no. 3, pp. 770–784, Jan. 2002.

[38] R. Perry and D. Green, *Perry’s chemical engineers’ handbook.*, 7th Editio. 2001.

[39] A. Turgut, I. Tavman, and S. Tavman, “Measurement of Thermal Conductivity of Edible Oils Using Transient Hot Wire Method,” *Int. J. Food Prop.*, vol. 12, no. 4, pp. 741–747, Jul. 2009.

[40] S. N. Sahasrabudhe, V. Rodriguez-Martinez, M. O’Meara, and B. E. Farkas, “Density, viscosity, and surface tension of five vegetable oils at elevated temperatures: Measurement and modeling,” *Int. J. Food Prop.*, vol. 20, no. sup2, pp. 1965–1981, Dec. 2017.

[41] O. O. Fasina and Z. Colley, “Viscosity and Specific Heat of Vegetable Oils as a Function of Temperature: 35°C to 180°C,” *Int. J. Food Prop.*, vol. 11, no. 4, pp. 738–746, Nov. 2008.

[42] “Therminol 66 Data Sheet.” .

[43] J. C. Maxwell, *A treatise on electricity and magnetism*. Clarendon Press, Oxford UK, 1873.

[44] W. Yu, E. V. Timofeeva, D. Singh, D. M. France, and R. K. Smith, “Investigations of heat transfer of copper-in-Therminol 59 nanofluids,” *Int. J. Heat Mass Transf.*, vol. 64, no. 1, pp. 1196–1204, 2013.

[45] N. Navarrete, L. Hernández, D. La Zara, J. R. Van Ommen, and R. Mondragón, “Nanoencapsulation of Metallic PCMs with Atomic Layer Deposition,” 2019.

[46] R. Martínez-Cuenca *et al.*, “Forced-convective heat-transfer coefficient and pressure drop of water-based nanofluids in a horizontal pipe,” *Appl. Therm. Eng.*, vol. 98, pp. 841–849, 2016.